JOURNAL OF GUIDANCE, CONTROL, AND DYNAMICS
Vol. 29, No. 4, July–August 2006

Airship Hover Stabilization Using a Backstepping Control Approach

José Raul Azinheira* and Alexandra Moutinho†
Instituto Superior Técnico, 1049-001 Lisbon, Portugal
and
Ely Carneiro de Paiva‡
Centro de Pesquisas Renato Archer, 13069-901 Campinas, SP, Brazil

The present paper introduces a novel approach for the airship hover stabilization problem. A synthetic modeling of the airship dynamics is introduced using a quaternion formulation of the kinematics equations. Based on this model, a backstepping design formulation is deduced for the aircraft hovering control. To deal with limitations caused by reduced actuation, saturations are introduced in the control design, and the global asymptotic stability of the system under saturation is demonstrated. The control objective is finally modified to cope with the strong lateral underactuation. Simulation results are presented for the hover stabilization of an unmanned robotic airship, with wind and turbulence conditions selected to demonstrate the behavior and robustness of the proposed solution.

Nomenclature

$a, b \in \mathbb{R}$	=	scalar tuning parameters
b_3, b_4	=	geometrical constants of the airship
$\boldsymbol{C}_3 \in \mathbb{R}^{3\times 3}$	=	matrix representing cross product $\boldsymbol{c}\times$
$\boldsymbol{c} \in \mathbb{R}^3$	=	c.g. coordinates in the local frame
$E \in \mathbb{R}$	=	East relative position of the airship
$\boldsymbol{F} \in \mathbb{R}^6$	=	vector of aerodynamic forces
$\boldsymbol{F}_u = [F_1, F_2, F_3]^T \in \mathbb{R}^3$	=	actuation input vector with force components only (longitudinal, lateral and vertical forces, respectively)
$\boldsymbol{f} = [\boldsymbol{F}_u^T, \boldsymbol{T}_u^T]^T \in \mathbb{R}^6$	=	force actuation input vector
$\boldsymbol{f}_s \in \mathbb{R}^6$	=	saturated force input vector
$\boldsymbol{g} \in \mathbb{R}^3$	=	gravity force vector given in Earth frame
$h \in \mathbb{R}$	=	airship altitude
$\boldsymbol{I}_n \in \mathbb{R}^{n\times n}$	=	identity matrix of size $n \times n$
$\boldsymbol{J}_a \in \mathbb{R}^{3\times 3}$	=	apparent inertia matrix of airship
$\boldsymbol{K} \triangleq -\boldsymbol{M}^{-1}\boldsymbol{\Omega}_6\boldsymbol{M} \in \mathbb{R}^{6\times 6}$	=	dynamic matrix associated with dynamics representation
k_1, k_2, k_3, k_5	=	second-order polynomials depending on airspeed V_t
l_4, l_6	=	geometrical constants of the airship
$\boldsymbol{M} \in \mathbb{R}^{6\times 6}$	=	full mass and inertia matrix of airship
$\boldsymbol{M}_a \in \mathbb{R}^{3\times 3}$	=	apparent mass matrix of airship
$m \in \mathbb{R}$	=	airship scalar mass
$m_w \in \mathbb{R}$	=	weighting mass of airship, as the difference between buoyancy mass and airship scalar mass
$N \in \mathbb{R}$	=	North relative position of the airship
$\boldsymbol{p} \in \mathbb{R}^3$	=	Cartesian coordinates of airship position error given in Earth frame
$\boldsymbol{Q} \in \mathbb{R}^{4\times 4}$	=	matrix relating the quaternions with their derivatives and angular velocities
$\boldsymbol{q} \in \mathbb{R}^4$	=	airship angular position error given in quaternion description
$\boldsymbol{S} \in \mathbb{R}^{3\times 3}$	=	transformation matrix from Earth frame to local frame
$T_D \in \mathbb{R}$	=	differential thrust of propellers (difference between left and right thrust)
$\boldsymbol{T}_u = [F_4, F_5, F_6]^T \in \mathbb{R}^3$	=	actuation input vector with torque inputs only (roll, pitch, and yaw torques, respectively)
$T_X \in \mathbb{R}$	=	total main propellers thrust
$T_Y \in \mathbb{R}$	=	stern propeller lateral thrust
$\boldsymbol{T} \triangleq \boldsymbol{DC} \in \mathbb{R}^{7\times 6}$	=	intermediate matrix for equation development
$\boldsymbol{T}^+ \in \mathbb{R}^{6\times 7}$	=	pseudoinverse of matrix $\boldsymbol{T}$
$\boldsymbol{U} = [T_X, \delta_v, T_D, T_Y, \delta_a, \delta_e, \delta_r]^T \in \mathbb{R}^7$	=	actuators input vector
$V_t \in \mathbb{R}$	=	true airspeed
$\boldsymbol{v} \in \mathbb{R}^3$	=	linear velocity vector in the local frame
$W, W_2 \in \mathbb{R}$	=	Lyapunov functions
$\boldsymbol{x} = [\boldsymbol{v}^T, \boldsymbol{\omega}^T]^T \in \mathbb{R}^6$	=	full airship inertial velocity vector given in local frame
$\boldsymbol{x}_e \in \mathbb{R}^6$	=	velocity error, as the difference between airship actual and reference velocities
$\boldsymbol{x}_w = [\boldsymbol{v}_w^T, \boldsymbol{\omega}_w^T]^T \in \mathbb{R}^6$	=	full wind velocity vector given in local frame
$\alpha, \beta \in \mathbb{R}$	=	angle of attack and sideslip angle
$\delta_a, \delta_e, \delta_r \in \mathbb{R}$	=	aileron, elevator, and rudder inputs from tail surfaces deflection
$\delta_v \in \mathbb{R}$	=	vectoring angle of main propellers
$\boldsymbol{\eta} = [\boldsymbol{p}^T, \boldsymbol{q}^T]^T \in \mathbb{R}^7$	=	airship position error given in Earth frame
$\boldsymbol{\eta}_e \in \mathbb{R}^7$	=	estimated airship position error between state and reference position, considering wind direction
$\boldsymbol{\Lambda} \in \mathbb{R}^{7\times 7}$	=	diagonal positive-definite matrix used as tuning parameter
$\lambda \in \mathbb{R}$	=	real scalar or matrix eigenvalue
$\rho \triangleq \sqrt{(a/b)} \in \mathbb{R}$	=	tuning parameter ratio
$\boldsymbol{\sigma}_1, \boldsymbol{\sigma}_2$	=	saturation functions

Received 25 April 2005; revision received 13 October 2005; accepted for publication 13 October 2005.

*Assistant Professor, Mechanical Engineering Department, Systems Group, IDMEC, Av. Rovisco Pais, 1.

†Teaching/Research Assistant, Mechanical Engineering Department, Systems Group, IDMEC, Av. Rovisco Pais, 1.

‡Research Engineer, Robotics and Computer Vision Department, DRVC/CenPRA, Rod. D. Pedro I, km 143.6.

$\phi, \theta, \psi \in \mathbb{R}$	=	Euler angles of the airship associated with transformation matrix $\boldsymbol{S}$
$\psi_w \in \mathbb{R}$	=	wind heading angle
$\boldsymbol{\Omega}_3 \in \mathbb{R}^{3\times 3}$	=	matrix representing cross product $\boldsymbol{\omega}\times$
$\boldsymbol{\Omega}_4 \in \mathbb{R}^{4\times 4}$	=	antisymmetric matrix associated with the angular velocity $\boldsymbol{\omega}$
$\boldsymbol{\omega} = [\omega_1, \omega_2, \omega_3]^T \in \mathbb{R}^3$	=	vector of airship angular speed given in local frame

I. Introduction

TECHNOLOGICAL advances and miniaturization in sensor, onboard processing, and communication systems lead to an increase in payload capacity and operational flexibility of unmanned aerial vehicles (UAVs), widening their potential use as observation and data-acquisition platforms in military, civil, and commercial scenarios. Although UAVs presently have a relatively small sharing in the aerospace market, their importance is expected to grow enormously in the next decades. UAVs (or a coordinated group of UAVS) are able to cover different application areas such as tactical reconnaissance and operational support; landmine detection; border, costal and remote regions patrol and monitoring; homeland security; law enforcement; search and rescue; operation in hazard or disaster zones; digital charting and mapping; mineral and archaeological prospecting; land-use survey for diagnosis, planning and management in rural and urban regions; agricultural and livestock studies, crop yield prediction; fire detection and firefighting management; global observing for environmental and climate research, including atmospheric and air quality, marine, limnological and forests monitoring and assessment; inspection of man-made structures such as pipelines, power transmission lines, dams and roads; transportation monitoring and control; communications and broadcast services; and others. Detailed UAVs applications scenarios and roadmaps are presented in Cox et al.[1] and Cambone et al.[2] from civil and military perspectives, respectively. For several of the just-mentioned applications, the UAV must often be able to sustain a quasi-stationary flight state (hover flight) over a certain target, independently of the perturbations introduced by the atmospheric conditions.

Different kinds of control techniques have been recently applied to solve the hovering problem of diverse types of UAVs. The automatic hovering of an outdoor autonomous airship using image-based visual servoing in a proportional derivative (PD) error feedback scheme was presented in Azinheira et al.[3] Linear robust multivariable control, fuzzy-logic control with evolutionary tuning, and nonlinear tracking control were the three control methodologies compared in Shim et al.[4] for an helicopter autopilot design. Also for hover control of an helicopter, Guo et al.[5] introduced a preliminary study on the use of neural adaptive control techniques, Yang and Liu[6] investigated the decoupling nonlinear H_∞ control design subject to model parameter uncertainties, and Mahony et al.[7] proposed a Lyapunov control design using backstepping techniques for an unmanned helicopter. Also based in this approach, Metni et al.[8] derived a visual servoing control law for UAV bridge inspection.

The present paper focus on a novel approach for the airship hover stabilization problem. It introduces a synthetic modeling of the airship dynamics, resulting in an original formulation of the system kinematics/dynamics with an appropriate change of variables allowing the application of backstepping techniques for the design of the UAV hover control. This work is an evolution over the previous linear-based controllers designed for the aerodynamic flight of the AURORA airship, including successful reports of lateral and longitudinal path tracking of the airship in real flight experiments.[9,10]

The backstepping approach[11] is a Lyapunov-based control design technique, usually applied in the control of nonlinear systems. By formulating a scalar positive function of the system states and then choosing a control law to make this function decrease, we have the guarantee that the nonlinear control system thus designed will be asymptotically stable and still robust to some unmatched uncertainties. Backstepping has been successfully applied in several applications of flight control.[12–14] Also addressing the issue of underactuated systems, this control technique has been applied in Beji et al.[15] and Toussaint et al.[16] The present paper describes the design of a backstepping control strategy that stabilizes the hovering flight of an airship, while being robust against perturbations (wind and turbulence) and unmatched dynamics.

The saturation of the control signals is also considered in the design because at low airspeeds or when in hovering state the airship is usually underactuated because of 1) reduced aerodynamic forces demanding a superior action by the engines for position and attitude control; 2) coupling of the main propellers that should provide forward and vertical forces at the same time (through the vectoring action of the thrusters); 3) absence of a lateral force actuator to oppose aerodynamic side forces; 4) level and rate saturation limits in the actuators; and 5) dynamics of the actuators limiting their time responses. All of these factors might lead to the saturation of the control signals, which are usually bounded. To cope with limitations caused by reduced actuation, we follow the idea of Teel,[17] which uses a nonlinear combination of saturation functions of linear feedbacks that globally stabilizes a chain of integrators. The problem of actuator limits is of fundamental interest for this kind of underactuated systems, making this a theoretical study closely related to practical applications. A similar approach was also applied with backstepping in Freeman and Praly[18] so that the boundedness of the control signals and its derivative were propagated through each step of the recursive design, while Metni et al.[8] follows the same idea for an UAV with orientation limitation.

In addition, we propose a guidance strategy to deal with the airship lateral underactuation in face of wind disturbances. A reference path from the current state to the desired state is defined as to minimize the need of lateral forces. Moreover, a yawing degree of freedom is introduced in the control objective, allowing the airship to align against the wind in the hovering condition. To evaluate the approach, representative simulation tests were performed, using the fully six-degrees-of-freedom nonlinear model-based simulation environment developed in the Aurora Project.[19] The simulations concern the hovering stabilization of the airship under low and high wind conditions and with possible inclusion of strong turbulence.

This paper is organized as follows. The airship modeling and backstepping design are presented in Sec. II. The inclusion of saturations in the control design is presented in Sec. III. The computation of the real actuators input and the lateral underactuation problem are considered in Sec. IV. Illustrative simulation results are presented in Sec. V, and finally some conclusions are drawn in Sec. VI.

II. Model and Control Design

A. Airship Dynamics Without Aerodynamic Forces

The original airship dynamics without aerodynamic forces,[20] considering the actuation as force and torque inputs $\boldsymbol{f} = (\boldsymbol{F}_u^T, \boldsymbol{T}_u^T)^T \in \mathbb{R}^6$, is

$$\begin{cases} \boldsymbol{M}_a\dot{\boldsymbol{\nu}} - m\boldsymbol{C}_3\dot{\boldsymbol{\omega}} = m\boldsymbol{\Omega}_3\boldsymbol{C}_3\boldsymbol{\omega} - \boldsymbol{\Omega}_3\boldsymbol{M}_a\boldsymbol{\nu} + m_w\boldsymbol{S}\boldsymbol{g} + \boldsymbol{F}_u \\ m\boldsymbol{C}_3\dot{\boldsymbol{\nu}} + \boldsymbol{J}_a\dot{\boldsymbol{\omega}} = -\boldsymbol{\Omega}_3\boldsymbol{J}_a\boldsymbol{\omega} - m\boldsymbol{\Omega}_3\boldsymbol{C}_3\boldsymbol{\nu} + m\boldsymbol{C}_3\boldsymbol{S}\boldsymbol{g} + \boldsymbol{T}_u \end{cases} \quad (1)$$

where $\boldsymbol{\nu} \in \mathbb{R}^3$ and $\boldsymbol{\omega} \in \mathbb{R}^3$ are the linear and angular velocity vectors in the local frame (centered at the airship center of volume), m is the airship mass, m_w is its weighting mass, $(\boldsymbol{M}_a \in \mathbb{R}^{3\times 3}, \boldsymbol{J}_a \in \mathbb{R}^{3\times 3})$ are the apparent linear and rotational inertia matrices, $\boldsymbol{S} \in \mathbb{R}^{3\times 3}$ is the unitary transformation matrix from Earth frame to local frame, and the synthetic matrix notation is used for the cross product:

$$\begin{cases} \boldsymbol{C}_3 = \boldsymbol{c}\times \\ \boldsymbol{\Omega}_3 = \boldsymbol{\omega}\times \end{cases}$$

with $\boldsymbol{C}_3 \in \mathbb{R}^{3\times 3}$, $\boldsymbol{\Omega}_3 \in \mathbb{R}^{3\times 3}$ and using $\boldsymbol{c} \in \mathbb{R}^3$ for the c.g. coordinates in the local frame. Manipulating the equations yields

$$\begin{bmatrix} \boldsymbol{M}_a & -m\boldsymbol{C}_3 \\ m\boldsymbol{C}_3 & \boldsymbol{J}_a \end{bmatrix} \begin{bmatrix} \dot{\boldsymbol{\nu}} \\ \dot{\boldsymbol{\omega}} \end{bmatrix} = -\begin{bmatrix} \boldsymbol{\Omega}_3\boldsymbol{M}_a & -m\boldsymbol{\Omega}_3\boldsymbol{C}_3 \\ m\boldsymbol{\Omega}_3\boldsymbol{C}_3 & \boldsymbol{\Omega}_3\boldsymbol{J}_a \end{bmatrix} \begin{bmatrix} \boldsymbol{\nu} \\ \boldsymbol{\omega} \end{bmatrix} + \begin{bmatrix} m_w\boldsymbol{S}\boldsymbol{g} \\ m\boldsymbol{C}_3\boldsymbol{S}\boldsymbol{g} \end{bmatrix} + \begin{bmatrix} \boldsymbol{F}_u \\ \boldsymbol{T}_u \end{bmatrix} \quad (2)$$

or

$$\begin{bmatrix} \boldsymbol{M}_a & -m\boldsymbol{C}_3 \\ m\boldsymbol{C}_3 & \boldsymbol{J}_a \end{bmatrix} \begin{bmatrix} \dot{\boldsymbol{v}} \\ \dot{\boldsymbol{\omega}} \end{bmatrix} = -\begin{bmatrix} \boldsymbol{\Omega}_3 & 0 \\ 0 & \boldsymbol{\Omega}_3 \end{bmatrix} \begin{bmatrix} \boldsymbol{M}_a & -m\boldsymbol{C}_3 \\ m\boldsymbol{C}_3 & \boldsymbol{J}_a \end{bmatrix} \begin{bmatrix} \boldsymbol{v} \\ \boldsymbol{\omega} \end{bmatrix} + \begin{bmatrix} m_w \boldsymbol{I}_3 \\ m\boldsymbol{C}_3 \end{bmatrix} \boldsymbol{S}\boldsymbol{g} + \begin{bmatrix} \boldsymbol{F}_u \\ \boldsymbol{T}_u \end{bmatrix} \tag{3}$$

or in concise form

$$\boldsymbol{M}\dot{\boldsymbol{x}} = -\boldsymbol{\Omega}_6 \boldsymbol{M}\boldsymbol{x} + \boldsymbol{E}\boldsymbol{S}\boldsymbol{g} + \boldsymbol{f} \tag{4}$$

where $\boldsymbol{x} = [\boldsymbol{v}^T \ \boldsymbol{\omega}^T]^T \in \mathbb{R}^6$ is the velocity state vector, $\boldsymbol{f}$ is the force input, $\boldsymbol{M} \in \mathbb{R}^{6\times 6}$ is a symmetric inertia matrix

$$\boldsymbol{\Omega}_6 \triangleq \begin{bmatrix} \boldsymbol{\Omega}_3 & 0 \\ 0 & \boldsymbol{\Omega}_3 \end{bmatrix} \in \mathbb{R}^{6\times 6}$$

and

$$\boldsymbol{E} \triangleq \begin{bmatrix} m_w \boldsymbol{I}_3 \\ m\boldsymbol{C}_3 \end{bmatrix} \in \mathbb{R}^{6\times 3}$$

If a modeling of the aerodynamic forces is to be considered, a new term must be introduced. This term is a function of the difference between the airship velocity and the wind velocity: $\boldsymbol{F} = \boldsymbol{F}(\boldsymbol{x} - \boldsymbol{x}_w)$. The aerodynamic forces are however more usually approximated as a function of the measured aerodynamic variables, with the airspeed V_t and aerodynamic angles, the angle of attack α and the sideslip angle β: $\boldsymbol{F} = \boldsymbol{F}(V_t, \alpha, \beta)$. Thus, the resulting model of the airship dynamics is given by

$$\boldsymbol{M}\dot{\boldsymbol{x}} = -\boldsymbol{\Omega}_6 \boldsymbol{M}\boldsymbol{x} + \boldsymbol{E}\boldsymbol{S}\boldsymbol{g} + \boldsymbol{F} + \boldsymbol{f} \tag{5}$$

B. Kinematics Modeling with Quaternions

Let the airship position error $\boldsymbol{\eta} = [\boldsymbol{p}^T \ \boldsymbol{q}^T]^T \in \mathbb{R}^7$ be described by its Cartesian coordinates $\boldsymbol{p} \in \mathbb{R}^3$ in an Earth frame and by a quaternion description $\boldsymbol{q} \in \mathbb{R}^4$ for its angular attitude.[21] The kinematics involves the transformation between velocity and position:

$$\begin{cases} \dot{\boldsymbol{p}} = \boldsymbol{S}^T \boldsymbol{v} \\ \dot{\boldsymbol{q}} = \frac{1}{2}\boldsymbol{Q}\begin{bmatrix} 0 \\ \boldsymbol{\omega} \end{bmatrix} \end{cases} \tag{6}$$

or

$$\dot{\boldsymbol{\eta}} = \begin{bmatrix} \boldsymbol{S}^T & 0 \\ 0 & \frac{1}{2}\boldsymbol{Q} \end{bmatrix} \boldsymbol{C}\boldsymbol{x} = \boldsymbol{D}\boldsymbol{C}\boldsymbol{x} = \boldsymbol{T}\boldsymbol{x} \tag{7}$$

where $\boldsymbol{Q} \in \mathbb{R}^{4\times 4}$ is the unitary matrix relating the quaternions with their derivatives and the angular rates

$$\boldsymbol{Q} = \begin{bmatrix} q_0 & -q_1 & -q_2 & -q_3 \\ q_1 & q_0 & -q_3 & q_2 \\ q_2 & q_3 & q_0 & -q_1 \\ q_3 & -q_2 & q_1 & q_0 \end{bmatrix} \tag{8}$$

with

$$\boldsymbol{C} \triangleq \begin{bmatrix} \boldsymbol{I}_3 & 0_3 \\ 0_{1,3} & 0_{1,3} \\ 0_3 & \boldsymbol{I}_3 \end{bmatrix} \in \mathbb{R}^{7\times 6}, \qquad \boldsymbol{D} \triangleq \begin{bmatrix} \boldsymbol{S}^T & 0 \\ 0 & \frac{1}{2}\boldsymbol{Q} \end{bmatrix} \in \mathbb{R}^{7\times 7}$$

and $\boldsymbol{T} \in \mathbb{R}^{7\times 6}$ is defined as $\boldsymbol{T} \triangleq \boldsymbol{D}\boldsymbol{C}$. The derivatives of the matrices in $\boldsymbol{D}$ are

$$\dot{\boldsymbol{S}} = -\boldsymbol{\Omega}_3 \boldsymbol{S} \Rightarrow \dot{\boldsymbol{S}}^T = \boldsymbol{S}^T \boldsymbol{\Omega}_3 \tag{9}$$

and

$$\dot{\boldsymbol{Q}} = \frac{1}{2}\boldsymbol{Q}\boldsymbol{\Omega}_4 \tag{10}$$

where $\boldsymbol{\Omega}_4 \in \mathbb{R}^{4\times 4}$ is an antisymmetric matrix associated with the angular velocity $\boldsymbol{\omega} = [\omega_1, \omega_2, \omega_3]^T$:

$$\boldsymbol{\Omega}_4 = \begin{bmatrix} 0 & -\omega_1 & -\omega_2 & -\omega_3 \\ \omega_1 & 0 & -\omega_3 & \omega_2 \\ \omega_2 & \omega_3 & 0 & -\omega_1 \\ \omega_3 & -\omega_2 & \omega_1 & 0 \end{bmatrix} \tag{11}$$

Defining

$$\boldsymbol{\Omega}_7 \triangleq \begin{bmatrix} \boldsymbol{\Omega}_3 & 0 \\ 0 & \frac{1}{2}\boldsymbol{\Omega}_4 \end{bmatrix} \in \mathbb{R}^{7\times 7}$$

leads to

$$\dot{\boldsymbol{D}} = \begin{bmatrix} \boldsymbol{S}^T\boldsymbol{\Omega}_3 & 0 \\ 0 & \frac{1}{4}\boldsymbol{Q}\boldsymbol{\Omega}_4 \end{bmatrix} = \begin{bmatrix} \boldsymbol{S}^T & 0 \\ 0 & \frac{1}{2}\boldsymbol{Q} \end{bmatrix} \begin{bmatrix} \boldsymbol{\Omega}_3 & 0 \\ 0 & \frac{1}{2}\boldsymbol{\Omega}_4 \end{bmatrix} = \boldsymbol{D}\boldsymbol{\Omega}_7 \tag{12}$$

The quaternion matrix $\boldsymbol{Q}$ is unitary ($\boldsymbol{Q}^T\boldsymbol{Q} = \boldsymbol{I}_4$), leading to another property of the matrix $\boldsymbol{T}$:

$$\boldsymbol{T}^T\boldsymbol{T} = \boldsymbol{C}^T \begin{bmatrix} \boldsymbol{S}^T & 0 \\ 0 & \frac{1}{2}\boldsymbol{Q} \end{bmatrix}^T \begin{bmatrix} \boldsymbol{S}^T & 0 \\ 0 & \frac{1}{2}\boldsymbol{Q} \end{bmatrix} \boldsymbol{C} = \boldsymbol{C}^T \begin{bmatrix} \boldsymbol{S}\boldsymbol{S}^T & 0 \\ 0 & \frac{1}{4}\boldsymbol{Q}^T\boldsymbol{Q} \end{bmatrix} \boldsymbol{C} = \begin{bmatrix} \boldsymbol{I}_3 & 0 \\ 0 & \frac{1}{4}\boldsymbol{I}_3 \end{bmatrix} \tag{13}$$

Finally, if we define the diagonal matrices $\boldsymbol{\Delta} \in \mathbb{R}^{6\times 6}$ and $\boldsymbol{\Delta}_7 \in \mathbb{R}^{7\times 7}$ as

$$\boldsymbol{\Delta} \triangleq \begin{bmatrix} \boldsymbol{I}_3 & 0 \\ 0 & \frac{1}{2}\boldsymbol{I}_3 \end{bmatrix} = (\boldsymbol{T}^T\boldsymbol{T})^{\frac{1}{2}} \tag{14}$$

$$\boldsymbol{\Delta}_7 \triangleq \begin{bmatrix} \boldsymbol{I}_3 & 0 \\ 0 & \frac{1}{2}\boldsymbol{I}_4 \end{bmatrix} = (\boldsymbol{D}^T\boldsymbol{D})^{\frac{1}{2}} \tag{15}$$

then we get

$$\boldsymbol{T}^T\boldsymbol{\Delta}_7^{-2}\boldsymbol{T} = \boldsymbol{\Delta}^{-2}\boldsymbol{T}^T\boldsymbol{T} = \boldsymbol{I}_6 \tag{16}$$

yielding two possible formulations for the left pseudo-inverse of $\boldsymbol{T}$:

$$\boldsymbol{T}^+ = \boldsymbol{T}^T\boldsymbol{\Delta}_7^{-2} = \boldsymbol{\Delta}^{-2}\boldsymbol{T}^T \tag{17}$$

C. Backstepping Controller Design

Gathering both the dynamic and cinematic equations leads to the system dynamics:

$$\dot{\boldsymbol{x}} = \boldsymbol{K}\boldsymbol{x} + \boldsymbol{M}^{-1}(\boldsymbol{E}\boldsymbol{S}\boldsymbol{g} + \boldsymbol{F} + \boldsymbol{f}), \qquad \dot{\boldsymbol{\eta}} = \boldsymbol{D}\boldsymbol{C}\boldsymbol{x}$$
$$\dot{\boldsymbol{S}} = -\boldsymbol{\Omega}_3\boldsymbol{S}, \qquad \dot{\boldsymbol{D}} = \boldsymbol{D}\boldsymbol{\Omega}_7 \tag{18}$$

where $\boldsymbol{K} \triangleq -\boldsymbol{M}^{-1}\boldsymbol{\Omega}_6\boldsymbol{M} \in \mathbb{R}^{6\times 6}$ is linearly dependent of the angular velocity $\boldsymbol{\omega}$, whereas $\boldsymbol{M}$ is constant or slowly varying with altitude (because the inertia terms depend on the air density). The desired stabilization corresponds to a control system objective where both the velocity $\boldsymbol{x}$ and the position error $\boldsymbol{\eta}$ are regulated to zero.

Consider two intermediate output variables $\boldsymbol{y}_1 \in \mathbb{R}^7$ and $\boldsymbol{y}_2 \in \mathbb{R}^6$:

$$\begin{cases} \boldsymbol{y}_1 = a\boldsymbol{\eta} + b\boldsymbol{T}\boldsymbol{x} \\ \boldsymbol{y}_2 = \boldsymbol{\Delta}\boldsymbol{x} \end{cases} \tag{19}$$

with two positive scalars (a, b), and let us define the tentative Lyapunov function

$$W = \frac{1}{2}\boldsymbol{y}_1^T\boldsymbol{y}_1 + \frac{1}{2}\boldsymbol{y}_2^T\boldsymbol{y}_2 \tag{20}$$

Then the derivative is

$$\dot{W} = \boldsymbol{y}_1^T\dot{\boldsymbol{y}}_1 + \boldsymbol{y}_2^T\dot{\boldsymbol{y}}_2 \tag{21}$$

where

$$\dot{\boldsymbol{y}}_1 = a\dot{\boldsymbol{\eta}} + b\dot{\boldsymbol{T}}\boldsymbol{x} + b\boldsymbol{T}\dot{\boldsymbol{x}} = a\boldsymbol{T}\boldsymbol{x} + b\boldsymbol{D}\boldsymbol{\Omega}_7\boldsymbol{C}\boldsymbol{x} + b\boldsymbol{T}\dot{\boldsymbol{x}}$$
$$\dot{\boldsymbol{y}}_2 = \boldsymbol{\Delta}\dot{\boldsymbol{x}} \tag{22}$$

leading to

$$\boldsymbol{y}_2^T\dot{\boldsymbol{y}}_2 = (\boldsymbol{\Delta}\boldsymbol{x})^T\boldsymbol{\Delta}\dot{\boldsymbol{x}} = \boldsymbol{x}^T\boldsymbol{\Delta}^2\dot{\boldsymbol{x}} = \boldsymbol{x}^T\boldsymbol{T}^T\boldsymbol{T}\dot{\boldsymbol{x}} \tag{23}$$

and finally

$$\dot{W} = (a\boldsymbol{\eta} + b\boldsymbol{T}\boldsymbol{x})^T(a\boldsymbol{T}\boldsymbol{x} + b\boldsymbol{D}\boldsymbol{\Omega}_7\boldsymbol{C}\boldsymbol{x} + b\boldsymbol{T}\dot{\boldsymbol{x}}) + (\boldsymbol{T}\boldsymbol{x})^T\boldsymbol{T}\dot{\boldsymbol{x}} \tag{24}$$

Then

$$\dot{W} = [a\boldsymbol{\eta} + (b+1/b)\boldsymbol{T}\boldsymbol{x}]^T(a\boldsymbol{T}\boldsymbol{x} + b\boldsymbol{D}\boldsymbol{\Omega}_7\boldsymbol{C}\boldsymbol{x} + b\boldsymbol{T}\dot{\boldsymbol{x}}) - [(1/b)\boldsymbol{T}\boldsymbol{x}]^T(a\boldsymbol{T}\boldsymbol{x} + b\boldsymbol{D}\boldsymbol{\Omega}_7\boldsymbol{C}\boldsymbol{x}) \tag{25}$$

If the input is chosen so that

$$b\boldsymbol{T}\dot{\boldsymbol{x}} = -\boldsymbol{\Lambda}[a\boldsymbol{\eta} + (b+1/b)\boldsymbol{T}\boldsymbol{x}] - a\boldsymbol{T}\boldsymbol{x} - b\boldsymbol{D}\boldsymbol{\Omega}_7\boldsymbol{C}\boldsymbol{x} \tag{26}$$

where $\boldsymbol{\Lambda} \in \mathbb{R}^{7\times 7}$ is a positive-definite matrix, then

$$\dot{W} = -[a\boldsymbol{\eta} + (b+1/b)\boldsymbol{T}\boldsymbol{x}]^T\boldsymbol{\Lambda}[a\boldsymbol{\eta} + (b+1/b)\boldsymbol{T}\boldsymbol{x}] - (1/b)(\boldsymbol{T}\boldsymbol{x})^T(a\boldsymbol{T}\boldsymbol{x} + b\boldsymbol{D}\boldsymbol{\Omega}_7\boldsymbol{C}\boldsymbol{x}) \tag{27}$$

or

$$\dot{W} = -[a\boldsymbol{\eta} + (b+1/b)\boldsymbol{T}\boldsymbol{x}]^T\boldsymbol{\Lambda}[a\boldsymbol{\eta} + (b+1/b)\boldsymbol{T}\boldsymbol{x}] - (a/b)(\boldsymbol{T}\boldsymbol{x})^T\boldsymbol{T}\boldsymbol{x} - \boldsymbol{x}^T\boldsymbol{C}^T\boldsymbol{\Delta}_7^2\boldsymbol{\Omega}_7\boldsymbol{C}\boldsymbol{x} \tag{28}$$

Taking into account that $\boldsymbol{\Delta}_7^2\boldsymbol{\Omega}_7$ is antisymmetric, which eliminates the last term, the derivative can finally be expressed as

$$\dot{W} = -[a\boldsymbol{\eta} + (b+1/b)\boldsymbol{T}\boldsymbol{x}]^T\boldsymbol{\Lambda}[a\boldsymbol{\eta} + (b+1/b)\boldsymbol{T}\boldsymbol{x}] - (a/b)(\boldsymbol{T}\boldsymbol{x})^T\boldsymbol{T}\boldsymbol{x} \tag{29}$$

which states that this derivative is negative definite ($\dot{W} < 0$) if $\boldsymbol{\Lambda} > 0$ and $a/b = \rho^2 > 0$, resulting then in a closed-loop system with global asymptotic stability. Although the Lyapunov function (21) is not directly a function of the state variables, it is easily verified that through the change of variables (19) the derivative of W only vanishes at the origin for $\boldsymbol{x} = 0$ and $\boldsymbol{\eta} = 0$.

1. Closed-Loop Dynamics

The closed-loop dynamics is then given by the control law definition

$$\boldsymbol{T}\dot{\boldsymbol{x}} = (1/b)\{-a\boldsymbol{\Lambda}\boldsymbol{\eta} - [a\boldsymbol{I}_7 + (b+1/b)\boldsymbol{\Lambda}]\boldsymbol{T}\boldsymbol{x} - b\boldsymbol{D}\boldsymbol{\Omega}_7\boldsymbol{C}\boldsymbol{x}\} \tag{30}$$

or

$$\begin{cases}\boldsymbol{T}\dot{\boldsymbol{x}} = -\left[\rho^2\boldsymbol{I}_7 + (1+1/b^2)\boldsymbol{\Lambda}\right]\boldsymbol{T}\boldsymbol{x} - \rho^2\boldsymbol{\Lambda}\boldsymbol{\eta} - \boldsymbol{D}\boldsymbol{\Omega}_7\boldsymbol{C}\boldsymbol{x}\\ \dot{\boldsymbol{\eta}} = \boldsymbol{T}\boldsymbol{x}\end{cases} \tag{31}$$

or, introducing $\boldsymbol{\Lambda}_1 \in \mathbb{R}^{7\times 7}$, such that $\boldsymbol{\Lambda}_1^2 = \rho^2\boldsymbol{I}_7 + (1+1/b^2)\boldsymbol{\Lambda}$,

$$\begin{cases}\dot{\boldsymbol{x}} = -\boldsymbol{T}^+\boldsymbol{\Lambda}_1^2\boldsymbol{T}\boldsymbol{x} - \rho^2\boldsymbol{T}^+\boldsymbol{\Lambda}\boldsymbol{\eta} - \boldsymbol{C}^T\boldsymbol{\Omega}_7\boldsymbol{C}\boldsymbol{x}\\ \dot{\boldsymbol{\eta}} = \boldsymbol{T}\boldsymbol{x}\end{cases} \tag{32}$$

The design parameters (ρ, b, $\boldsymbol{\Lambda}$), respectively two positive scalars and a positive-definite matrix, are tuning parameters, used to adjust the closed-loop characteristics, by instance in order to avoid exciting the unmodeled dynamics.

2. Control Law

The control law is deduced from Eqs. (18) and (32)

$$\boldsymbol{K}\boldsymbol{x} + \boldsymbol{M}^{-1}(\boldsymbol{E}\boldsymbol{S}\boldsymbol{g} + \boldsymbol{F} + \boldsymbol{f}) = -\boldsymbol{T}^+\boldsymbol{\Lambda}_1^2\boldsymbol{T}\boldsymbol{x} - \rho^2\boldsymbol{T}^+\boldsymbol{\Lambda}\boldsymbol{\eta} - \boldsymbol{C}^T\boldsymbol{\Omega}_7\boldsymbol{C}\boldsymbol{x} \tag{33}$$

leading to

$$\boldsymbol{f} = \boldsymbol{M}\left(-\boldsymbol{T}^+\boldsymbol{\Lambda}_1^2\boldsymbol{T}\boldsymbol{x} - \rho^2\boldsymbol{T}^+\boldsymbol{\Lambda}\boldsymbol{\eta} - \boldsymbol{C}^T\boldsymbol{\Omega}_7\boldsymbol{C}\boldsymbol{x} - \boldsymbol{K}\boldsymbol{x}\right) - \boldsymbol{E}\boldsymbol{S}\boldsymbol{g} - \boldsymbol{F} \tag{34}$$

or

$$\boldsymbol{f} = -\boldsymbol{M}\boldsymbol{T}^+\left(\rho^2\boldsymbol{\Lambda}\boldsymbol{\eta} + \boldsymbol{\Lambda}_1^2\boldsymbol{T}\boldsymbol{x}\right) - \boldsymbol{M}(\boldsymbol{C}^T\boldsymbol{\Omega}_7\boldsymbol{C} + \boldsymbol{K})\boldsymbol{x} - \boldsymbol{E}\boldsymbol{S}\boldsymbol{g} - \boldsymbol{F} \tag{35}$$

To cope with limitations caused by the model approximations or to reduced actuation, it is interesting or even necessary to investigate the possibility of introducing saturations into the control design, which shall be considered in the next section.

III. Control Saturation

To include the input limitations into the design phase, the control law (35) was adapted with the inclusion of saturations in the feedback law according to the definitions introduced in the Appendix. Assuming that matrix $\boldsymbol{\Lambda}$ is diagonal, Eq. (35) can be written as

$$\boldsymbol{f} = -\boldsymbol{M}\boldsymbol{A}^T(\boldsymbol{A}\boldsymbol{x} + \boldsymbol{\Gamma}\boldsymbol{x} + \boldsymbol{B}\boldsymbol{\eta}) - \boldsymbol{E}\boldsymbol{S}\boldsymbol{g} - \boldsymbol{F} \tag{36}$$

where

$$\boldsymbol{A} \triangleq \boldsymbol{\Delta}_7^{-1}\boldsymbol{\Lambda}_1\boldsymbol{T} \in \mathbb{R}^{7\times 6}, \qquad \boldsymbol{B} \triangleq \rho^2\boldsymbol{\Delta}_7^{-1}\boldsymbol{\Lambda}_1^{-1}\boldsymbol{\Lambda} \in \mathbb{R}^{7\times 7}$$
$$\boldsymbol{\Gamma} \triangleq \boldsymbol{\Lambda}_1^{-1}\boldsymbol{\Delta}_7^{-1}\boldsymbol{T}\left(\boldsymbol{C}^T\boldsymbol{\Omega}_7\boldsymbol{C} + \boldsymbol{K}\right) \in \mathbb{R}^{7\times 6} \tag{37}$$

Let us now introduce saturation functions $\boldsymbol{\sigma}_1$ and $\boldsymbol{\sigma}_2$ (the appendix), respectively, on $\boldsymbol{B}\boldsymbol{\eta}$ and $\boldsymbol{A}\boldsymbol{x}$,

$$\boldsymbol{f}_s = -\boldsymbol{M}\boldsymbol{A}^T\boldsymbol{\sigma}_2[\boldsymbol{A}\boldsymbol{x} + \boldsymbol{\Gamma}\boldsymbol{x} + \boldsymbol{\sigma}_1[\boldsymbol{B}\boldsymbol{\eta}]] - \boldsymbol{E}\boldsymbol{S}\boldsymbol{g} - \boldsymbol{F} \tag{38}$$

Looking for the stability of the velocity state, let us define $W_2 = \frac{1}{2}\boldsymbol{x}^T\boldsymbol{x}$. Considering the saturated force input (38), the velocity derivative (18) is now

$$\dot{\boldsymbol{x}} = \boldsymbol{K}\boldsymbol{x} + \boldsymbol{M}^{-1}(\boldsymbol{E}\boldsymbol{S}\boldsymbol{g} + \boldsymbol{F} + \boldsymbol{f}_s) \tag{39}$$

or

$$\dot{\boldsymbol{x}} = \boldsymbol{K}\boldsymbol{x} - \boldsymbol{A}^T\boldsymbol{\sigma}_2[\boldsymbol{A}\boldsymbol{x} + \boldsymbol{\Gamma}\boldsymbol{x} + \boldsymbol{\sigma}_1[\boldsymbol{B}\boldsymbol{\eta}]] \tag{40}$$

leading to

$$\dot{W}_2 = \boldsymbol{x}^T\boldsymbol{K}\boldsymbol{x} - \boldsymbol{x}^T\boldsymbol{A}^T\boldsymbol{\sigma}_2[\boldsymbol{A}\boldsymbol{x} + \boldsymbol{\Gamma}\boldsymbol{x} + \boldsymbol{\sigma}_1[\boldsymbol{B}\boldsymbol{\eta}]] \tag{41}$$

The first term is zero because $\boldsymbol{K}$ is antisymmetric and, introducing $\boldsymbol{z}_1 \triangleq \boldsymbol{B}\boldsymbol{\eta} \in \mathbb{R}^7$, $\boldsymbol{z}_2 \triangleq \boldsymbol{A}\boldsymbol{x} \in \mathbb{R}^7$ and $\boldsymbol{v}_2 \triangleq \boldsymbol{\Gamma}\boldsymbol{x} \in \mathbb{R}^7$, the equation can be written as

$$\dot{W}_2 = -\boldsymbol{z}_2^T\boldsymbol{\sigma}_2[\boldsymbol{z}_2 + \boldsymbol{v}_2 + \boldsymbol{\sigma}_1[\boldsymbol{z}_1]] \tag{42}$$

If the saturations are chosen so that $R_1 < \frac{1}{2}r_2$, then, using Theorem 2 (the appendix) and its corollary, it can be deduced that for $|\boldsymbol{z}_2| > \frac{1}{2}r_2$, $\dot{W}_2 < 0$, showing that W_2 is a Lyapunov function. Therefore, after a finite time T_2 the variable $\boldsymbol{z}_2$ will enter the linear zone of its saturation and remain in it. After time T_2, the force input is then

$$\boldsymbol{f}_s = -\boldsymbol{M}\boldsymbol{A}^T(\boldsymbol{A}\boldsymbol{x} + \boldsymbol{\Gamma}\boldsymbol{x} + \boldsymbol{\sigma}_1[\boldsymbol{B}\boldsymbol{\eta}]) - \boldsymbol{E}\boldsymbol{S}\boldsymbol{g} - \boldsymbol{F} \tag{43}$$

and the velocity derivative is

$$\dot{\boldsymbol{x}} = \boldsymbol{K}\boldsymbol{x} - \boldsymbol{A}^T(\boldsymbol{A}\boldsymbol{x} + \boldsymbol{\Gamma}\boldsymbol{x} + \boldsymbol{\sigma}_1[\boldsymbol{B}\boldsymbol{\eta}]) \tag{44}$$

$$= -\boldsymbol{T}^+\left[\rho^2\boldsymbol{T}\boldsymbol{x} + (1+1/b^2)\boldsymbol{\Lambda}\boldsymbol{T}\boldsymbol{x} + \boldsymbol{D}\boldsymbol{\Omega}_7\boldsymbol{C}\boldsymbol{x} + \boldsymbol{\sigma}_1[\rho^2\boldsymbol{\Lambda}\boldsymbol{\eta}]\right] \tag{45}$$

leading to the saturated version of Eq. (26):

$$b\boldsymbol{T}\dot{\boldsymbol{x}} = -\boldsymbol{\Lambda}[\boldsymbol{\sigma}_1[a\boldsymbol{\eta}] + (b+1/b)\boldsymbol{T}\boldsymbol{x}] - a\boldsymbol{T}\boldsymbol{x} - b\boldsymbol{D}\boldsymbol{\Omega}_7\boldsymbol{C}\boldsymbol{x} \tag{46}$$

Recalling now the overall function $W = \frac{1}{2}\boldsymbol{y}_1^T\boldsymbol{y}_1 + \frac{1}{2}\boldsymbol{y}_2^T\boldsymbol{y}_2$, we can rewrite Eq. (29) with the saturation as

$$\dot{W} = -[a\boldsymbol{\eta} + (b + 1/b)\boldsymbol{Tx}]^T\boldsymbol{\Lambda}[\boldsymbol{\sigma}[a\boldsymbol{\eta}] + (b + 1/b)\boldsymbol{Tx}] - (a/b)(\boldsymbol{Tx})^T\boldsymbol{Tx} \tag{47}$$

or even

$$\dot{W} = -(\boldsymbol{X}_2\boldsymbol{z}_2 + \boldsymbol{X}_1\boldsymbol{z}_1)^T(\boldsymbol{X}_2\boldsymbol{z}_2 + \boldsymbol{X}_1\boldsymbol{\sigma}_1[\boldsymbol{z}_1]) - \rho^2(\boldsymbol{Tx})^T(\boldsymbol{Tx}) \tag{48}$$

with $\boldsymbol{z}_1 = \boldsymbol{B\eta} \in \mathbb{R}^7$, $\boldsymbol{z}_2 = \boldsymbol{Ax} \in \mathbb{R}^7$ as previously defined, and $\boldsymbol{X}_1 \in \mathbb{R}^{7\times 7}$ and $\boldsymbol{X}_2 \in \mathbb{R}^{7\times 7}$ as

$$\boldsymbol{X}_2 \triangleq b(1 + 1/b^2)\boldsymbol{\Delta}_7\boldsymbol{\Lambda}_1^{-1}\boldsymbol{\Lambda}^{\frac{1}{2}} = b(1 + 1/b^2)\boldsymbol{\Delta}_7\left[\rho^2\boldsymbol{\Lambda}^{-1} + (1 + 1/b^2)\boldsymbol{I}_7\right]^{-\frac{1}{2}}$$

$$\boldsymbol{X}_1 \triangleq b\boldsymbol{\Delta}_7\boldsymbol{\Lambda}_1\boldsymbol{\Lambda}^{-\frac{1}{2}} = b\boldsymbol{\Delta}_7\left[\rho^2\boldsymbol{\Lambda}^{-1} + (1 + 1/b^2)\boldsymbol{I}_7\right]^{\frac{1}{2}} \tag{49}$$

From the preceding formulas, and considering that all of the design parameters are positive, it can be verified that both $\boldsymbol{X}_1$ and $\boldsymbol{X}_2$ are positive diagonal matrices and that their minimum and maximum eigenvalues verify

$$\lambda_{\max}(\boldsymbol{X}_2) < b(1 + 1/b^2)^{\frac{1}{2}} < \lambda_{\min}(\boldsymbol{X}_1) \tag{50}$$

which leads to

$$|\boldsymbol{z}_2| < |\boldsymbol{\sigma}_1[\boldsymbol{z}_1]| \Rightarrow |\boldsymbol{X}_2\boldsymbol{z}_2| < |\boldsymbol{X}_1\boldsymbol{\sigma}_1[\boldsymbol{z}_1]| \tag{51}$$

Then, using theorem 3 (the appendix) shows that if $|\boldsymbol{\sigma}_1[\boldsymbol{z}_1]| \geq r_1$, $\dot{W} < 0$, and otherwise, $\boldsymbol{\sigma}_1[\boldsymbol{z}_1] = \boldsymbol{z}_1$, and clearly we also have $\dot{W} < 0$, finally showing the exponential stability of the controlled system.

IV. Using the Airship Actuators

A. Airship Actuators

The available actuators of any airship are not likely to provide a full controllability as the preceding control design would request. To a higher extent than for other air vehicles, the airship is an underactuated system, and the control design must be carefully adapted, as well as the allowable requirements. In the sequel, the case of the Aurora AS800B airship will be considered. The control actuators of the airship can be split into two sets (Fig. 1):

1) Force inputs are available from the vectored two main propellers, on each side of the gondola (vectoring ranging from −30 to +120 deg). The propellers provide a complementary lift to oppose the weighting mass, as well as a forward thrust controlling the longitudinal speed; when a differential input is added between the two propellers (meaning different rotations for the left and right engines), they also provide torque to control the rolling motion near hover; finally, a stern lateral thruster might be necessary to provide yaw control at low airspeeds, although it has not been used in the Aurora airship standard configuration.

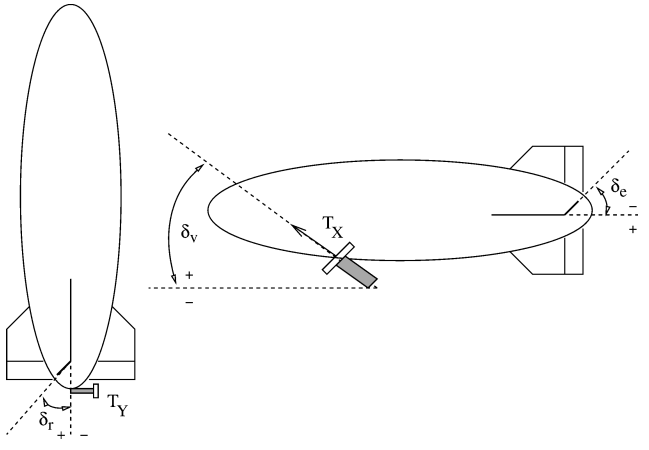

Fig. 1 Airship actuators.

2) Surface deflections of the tail (in the range of −25 to +25 deg) in the presence of a minimum airspeed provide torque inputs mostly for the control of the pitching and yawing motions. However, when the air is perfectly still and no wind is available, the hover control is reduced to the use of the force inputs only.

Thus, the real airship actuators input is given by $[T_X, \delta_v, T_D, T_Y, \delta_a, \delta_e, \delta_r]^T$, where T_X is the total main propellers thrust; δ_v is the vectoring angle; T_D is the difference between right and left thrust; T_Y is the stern propeller lateral thrust, and $\delta_a, \delta_e, \delta_r$ are the tail surfaces deflections, corresponding to aileron, elevator and rudder, respectively. The aileron input δ_a is generated through the opposite deflection of each of the fins yielding a rolling moment.

B. Control Allocation

1. Force Inputs

The relation between force actuators and force inputs will then be as follows:

1) Near hover, the two main propellers correspond to three inputs (T_X, δ_v, T_D)—total thrust, vectoring angle, and differential thrust—providing longitudinal and vertical force and pitching and rolling torques.

2) If available, the tail lateral thruster adds one input T_Y, providing a side force and a yawing motion.

These force actuators are slightly influenced by the airspeed but can be considered as independent in a first step.

2. Surface Deflections

The action from the surface deflections is, on the contrary, a function of the dynamic pressure and varies as the square of the airspeed V_t, according to the aerodynamic characteristics of the airship[21]. The surface deflections correspond to the three standard inputs of aileron, elevator, and rudder deflections, represented respectively by $(\delta_a, \delta_e, \delta_r)$. As just listed, with seven inputs to control six forces (three forces and three torques), the airship might seem overactuated, but several limitations severely reduce the controllability:

1) The stern thruster only provides a yawing torque, and its lateral force is negligible, so that no actuator is really available to oppose the aerodynamic side force.

2) The main propellers provide four coupled force components with only three inputs.

3) The tail surfaces depend on the airspeed, and their authority vanishes in the no-wind case, leaving the airship to be controlled by the force inputs only.

4) All of the actuators have level and rate saturation limits, so that might not be avoided.

5) The force actuators in particular have their own dynamics, with limited response times, that must be taken into account.

To reduce the influence of these limitations, the solution adopted in the control design was to add the tuning parameters $(\rho, b, \boldsymbol{\Lambda})$, so as to decrease the closed-loop frequency, searching for a slower solution, that would be more robust to the unmodeled and approximate dynamics, as well as input saturations.

3. Airship Inputs

The relation from actuators to force inputs can then be established in an approximated approach neglecting the actuators dynamics, using the airspeed measurement and resolving the possible redundancies according to the usual operation of the airship:

$$\boldsymbol{U} = \boldsymbol{U}(\boldsymbol{f}, V_t) \tag{52}$$

where $\boldsymbol{U} = [T_X, \delta_v, T_D, T_Y, \delta_a, \delta_e, \delta_r]^T \in \mathbb{R}^7$ is the real actuators input. (The airship aerodynamic angles also have their effect, but they can be neglected in a first step, assuming small incidence angles.) In the present case, the input $\boldsymbol{U}$ is computed as solution of the following system:

$$f_1 = T_X\cos(\delta_v) + k_1\delta_e, \qquad f_2 = -k_2\delta_r$$

$$f_3 = -T_X\sin(\delta_v) + k_3\delta_e, \qquad f_4 = k_2l_4\delta_a + b_4\sin(\delta_v)T_D$$

$$f_5 = T_Xb_3\cos(\delta_v) + k_5\delta_e, \qquad f_6 = k_2l_6\delta_r + b_4\cos(\delta_v)T_D$$

where (b_j, l_j) are geometrical constants of the airship and $k_j(V_t)$ are second-order polynomials expressing the airspeed depending authority of the tail actuators.

C. Dealing with the Lateral Underactuation

For a hovering objective with respect to the ground or a ground target, the wind disturbance appears both as a positive factor, which will help to control the airship thanks to the increased tail authority; and a drawback, producing a mostly horizontal force, that needs to be balanced by an airship actuator, and this is only possible using the longitudinal forces and aligning the airship to reduce the lateral actuation. As a consequence, and in order to avoid the saturation occurrences resulting from the reduced lateral controllability, along with the definition of suitable saturation limits, it is necessary to correct the control objective, and in the presence of wind, it is necessary to 1) allow a yawing degree of freedom, so that the airship can align against the wind and the lateral force input can vanish in stationary conditions; and 2) define a reference path from the current state to the desired state that will reduce the need of lateral forces to a low and acceptable value.

The feedback law (38) expressed earlier must be adapted to the tracking case

$$\boldsymbol{f}_s = -\boldsymbol{M}\boldsymbol{A}^T\boldsymbol{\sigma}_2[(\boldsymbol{A}+\boldsymbol{\Gamma})\boldsymbol{x}_e + \boldsymbol{\sigma}_1[\boldsymbol{B}\boldsymbol{\eta}_e]] - \boldsymbol{E}\boldsymbol{S}\boldsymbol{g} - \boldsymbol{F} \tag{53}$$

where the feedback is now in terms of position $\boldsymbol{\eta}_e$ and velocity $\boldsymbol{x}_e$ errors, between state and a reference position and velocity path. State error computation is done as follows: 1) wind heading estimation ψ_w, using the measurement of the airship position as well as airspeed and sideslip angle; 2) compute the relative Cartesian position error after a rotation with angle ψ_w around target position; 3) reference shaping, computing a yaw reference for first-order lateral regulation, and then a yaw-rate reference in agreement with the yaw reference; and 4) compute quaternion error using computed yaw reference. Comparing to the control solution previously presented, it shall be assumed that the reference path varies slowly and that its derivative can be neglected when compared to the state derivative. (This also means that the wind mean value is assumed as slowly varying.)

V. Simulation Results

To evaluate the approach, repetitive simulation tests were performed, using the fully nonlinear platform developed in the Aurora project[10,19] to simulate the motion of an airship prototype weighting 33 kg and with a volume of 30 m^3 (Fig. 2). The simulation results presented here concern a hovering stabilization of the airship at ($N = 0$ m, $E = 0$ m) and constant altitude and from an initial horizontal error ($N_i = -25$ m, $E_i = 5$ m), where N and E stand for the North and East relative position. For illustrative purposes, the attitude of the airship is also set out of equilibrium, with 10 deg in all Euler angles. Two extreme cases are considered, allowing the enhancement of the effect of the underactuation aspect: 1) a fully actuated airship (case FA), where the airship is assumed to accept as input the six-dimensional force vector as generated by the initial control law [Eq. (35)]; and 2) real actuators (case RA), where the actual nonlinear model of the airship is used, with the real actuator models as control inputs.

Fig. 2 AURORA AS800B airship.

A. Nominal Wind

The nominal case corresponds to a hovering stabilization in a constant wind blowing from North at 3 m/s. The position variables are presented in Fig. 3, with the horizontal North–East path on top, then the Cartesian coordinates (North, East, and altitude) and the Euler angles. (The attitude is here presented in terms of the Euler angles, which are more meaningful and intuitive than the quaternions.) The results with full actuation are on the left, and the real actuators' case is on the right. For the latter case, the saturations used correspond to the following force maxima: $[F_1, F_2, F_3, F_4, F_5, F_6] = [107, 13, 40, 27, 267, 27](N)$. The first clear difference is in the horizontal path, where the FA case is nearly a straight line, whereas for the RA case the reference shaping leads to a priority to the alignment of the airship against the wind, and then reaches the desired position. The saturations associated with the RA case are also quite obvious in the North and East time curves, namely, a saturated rate on the North curve and some oscillation on the East one, while the FA curves exhibit a first-order response. The result is a slightly higher settling time, with around 15 s for the FA case and 20 s for the RA case. The Euler angles look more dissimilar, slow and smooth in the FA case, more oscillating but faster in the RA case: this is clearly again the result of the reference shaping, demanding a faster angular stabilization in order to reduce the need for lateral force inputs.

The lateral and yaw correction is also coupled with the rolling motion, and this coupling is increased by the airship aerodynamics. To evaluate the effect of this aerodynamic disturbance, the aerodynamic variables are shown in Fig. 4, with the FA case on the left and the RA case on the right. The airspeed V_t is presented on the top curve, followed by the angle of attack α and sideslip angle β. In the FA case, the airspeed climbs up to 8 m/s, before settling to its nominal value of 3 m/s: with 8 m/s the aerodynamic forces can hardly be neglected, and the airship would fly without any vectoring. In the RA case, the airspeed only goes up to 4.5 m/s, remaining there during most of the correction. The aerodynamic angles also show smaller values in the RA case. Figure 5 presents the force inputs generated by the control law, with the FA case on the left and the RA on the right. The saturation levels are clearly visible in the RA case, reducing the initial peaks, that exhibit very high values in the FA case; a saturated zone is then shown by the RA case from 7 to 18 s (saturation attained in F_2 is propagated to some of the other forces), followed by the final stabilization. The actuator inputs in the RA case are presented in Fig. 6, with the longitudinal inputs on the left and the lateral inputs on the right. After an initial correction, mostly present in the longitudinal actuators, the lateral correction is naturally mostly controlled by the lateral actuators.

B. Small Wind Example

As it was already explained, when the aerodynamic forces are reduced, with a smaller mean wind speed by instance, the control surfaces have less authority, which namely makes the lateral control of the airship quite a difficult issue. The behavior of the control system in such a case is presented in Fig. 7, corresponding to the nominal given conditions except for a wind speed reduced to only 1 m/s. When compared to the nominal case above in the 3-m/s wind speed case, the lateral alignment is much slower, whereas the longitudinal control is mostly similar. The difference between the lateral and longitudinal behavior is clearly shown in the horizontal path, with a final approach from the south with 3 m/s, whereas the approach is from east in the 1-m/s one. The reason for the lateral higher sensitivity to the wind intensity is that the longitudinal motion is mostly controlled by the force inputs, whereas the lateral one is mostly depending on the rudder deflection input to control the yaw angle and the lateral position. The airspeed climbs up only to 2.2 m/s, but most of the lateral correction is performed with only 1-m/s airspeed, which explains the higher settling time.

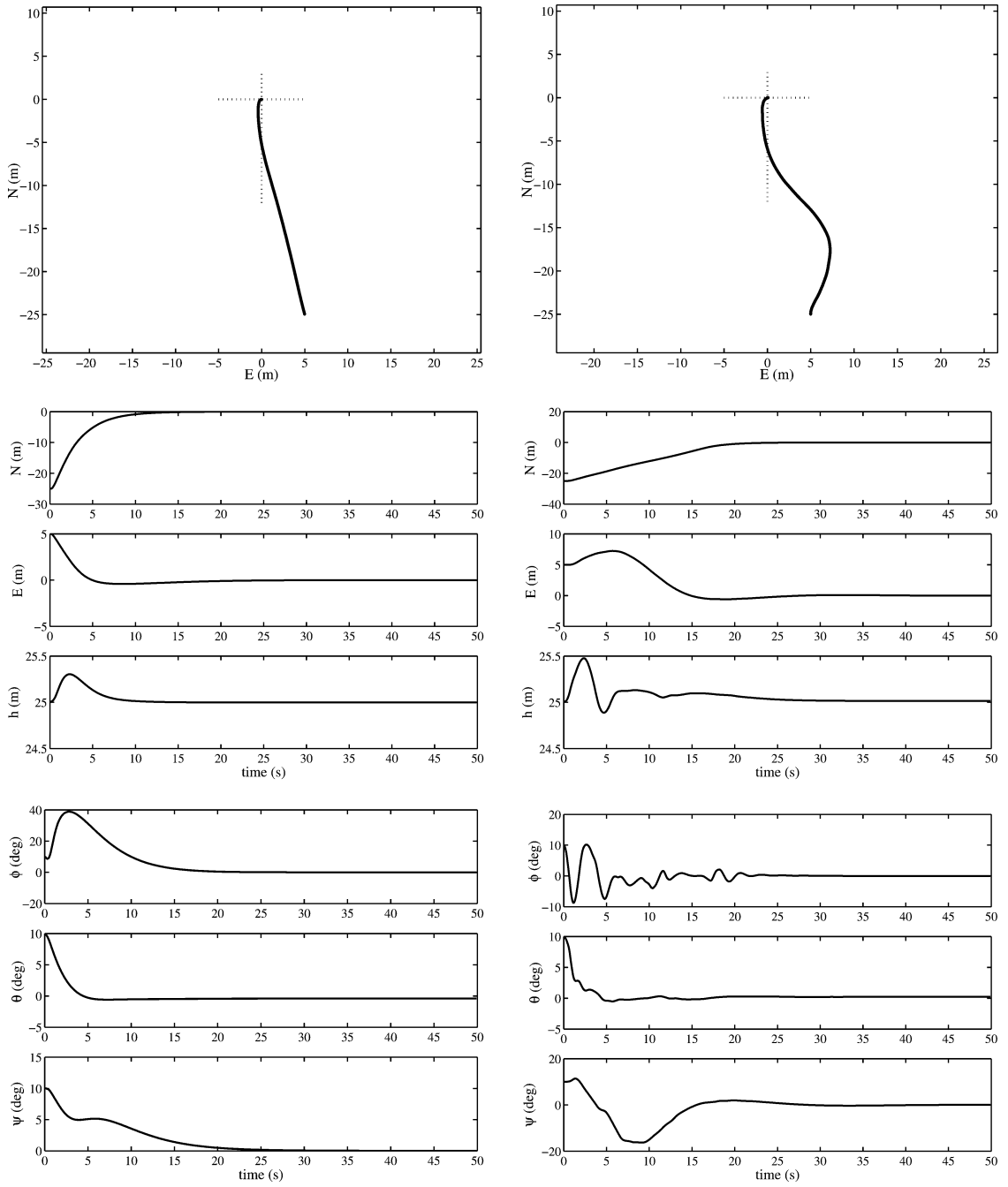

Fig. 3 Nominal case, position variables: $N - E$ path, $N, E, h, \phi, \theta, \psi$: left, FA case; and right, RA case.

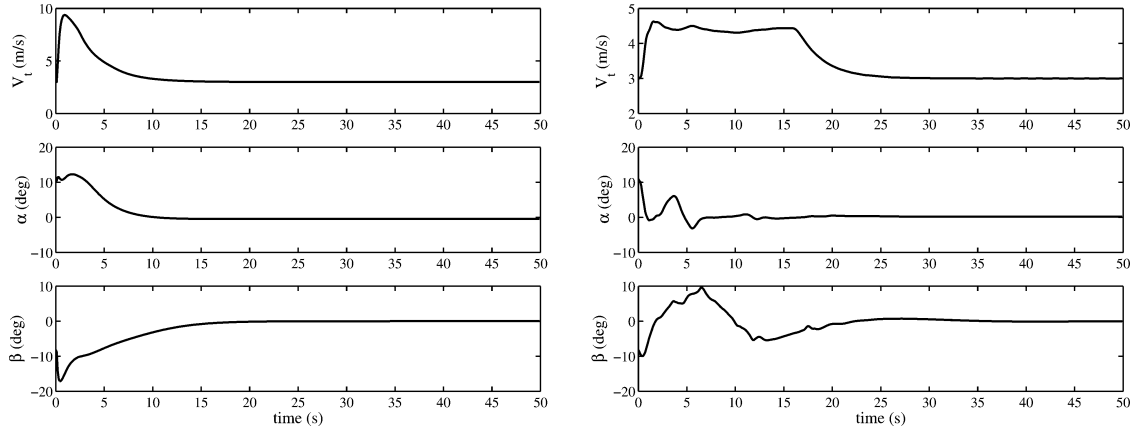

Fig. 4 Aerodynamic variables V_t, α, β: left, FA case; and right, RA case.

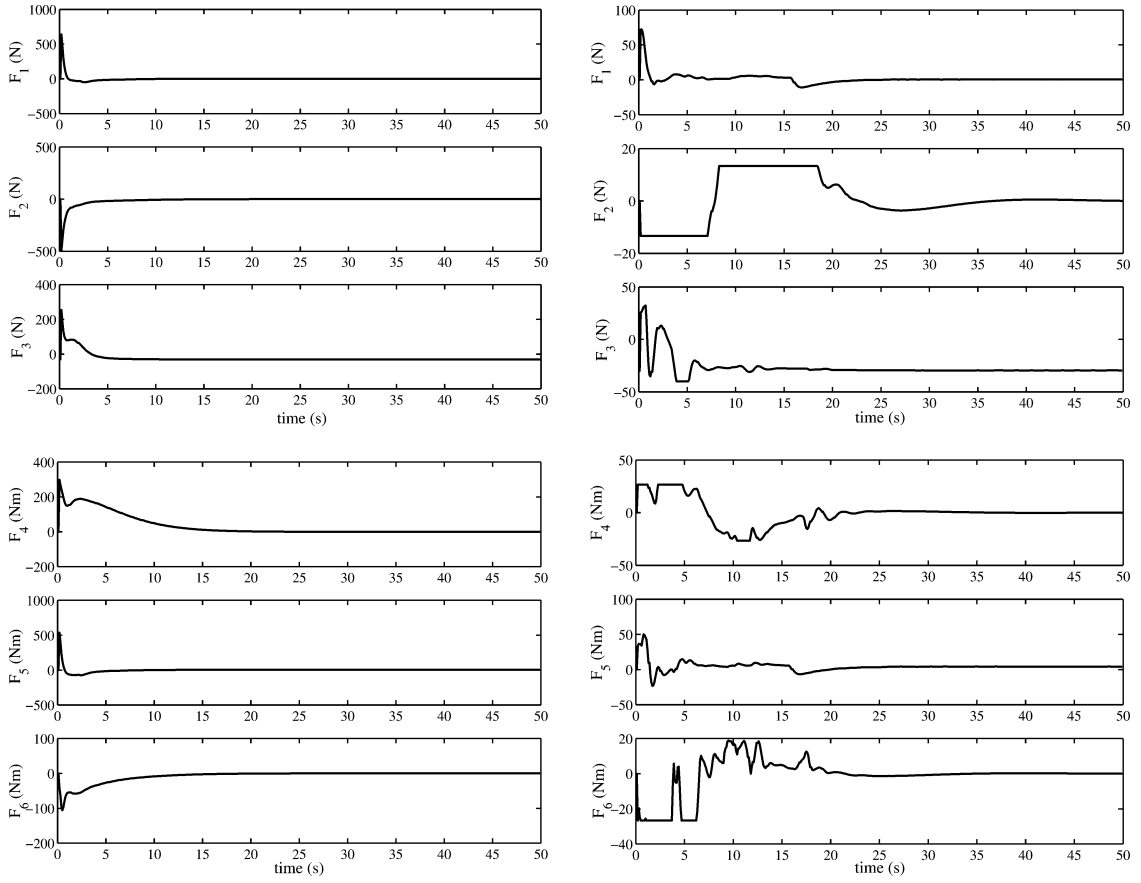

Fig. 5 Force demands: left, FA case; and right, RA case.

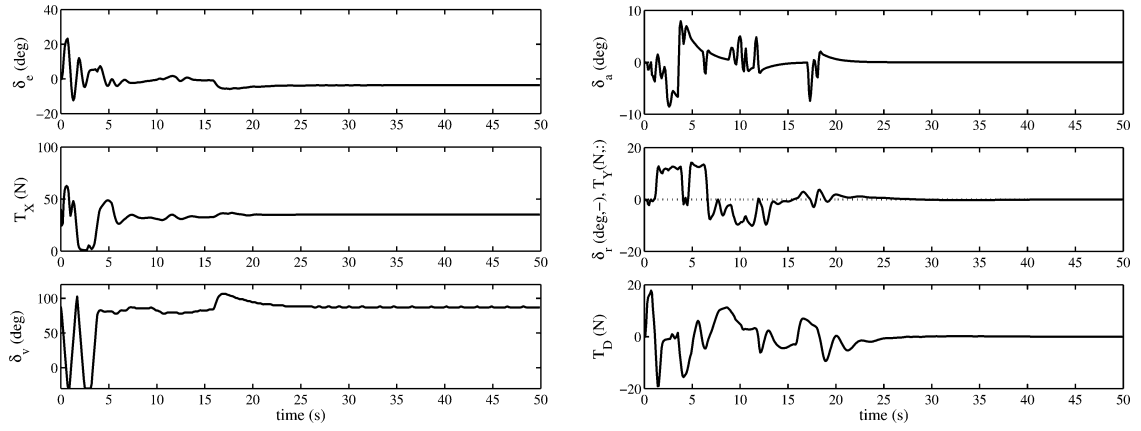

Fig. 6 Real actuator case inputs.

C. Nominal Wind Plus Turbulence

To evaluate the airship control behavior in a more realistic example, a simulation was run with the nominal conditions, but with a turbulent wind corresponding to a mean windspeed of 3 m/s from North and a continuous atmospheric turbulence with 3-m/s intensity. (In the Aurora AS800B simulation platform, the continuous atmospheric turbulence is modelled with a Dryden model.) This is an intermediate condition with a relatively high turbulence, with wind heading changes reaching 40 deg, but one can consider the airship should be able to stabilize a hover in these conditions, for ground or target observation. As to make a better analysis of the turbulence input response, the simulation time was increased to 150 s. The results from this simulation in the RA case are presented in Fig. 8. Comparing with the nominal curves (Figs. 3, 4, and 6), the horizontal path allows us to verify that the initial alignment is very similar, and then, when the airship reaches the target point, the wind input results in a mostly lateral oscillation around 2 m wide. The influence of the turbulence disturbance is obviously particularly visible for the aerodynamic variables, with airspeed oscillations above 1 m/s, the aerodynamic angles going up to almost 15 deg. The longitudinal control is however quite good, suffering very little from the disturbance. The lateral control is more difficult, which is simply explained by the high aerodynamic lateral forces caused by the wind inputs, being the airship clearly underactuated in this axis. The overall stabilization objective is still achieved, and namely the roll and pitch angles are very well regulated. In terms of control inputs, the rudder deflection δ_r and the differential thrust T_D are the more active inputs, necessary to oppose the lateral forces and rolling torques.

A quantitative measurement of the control performance can be obtained from the rms measurement of the last 100 s by instance (approximately equivalent to the stabilized region), leading to the

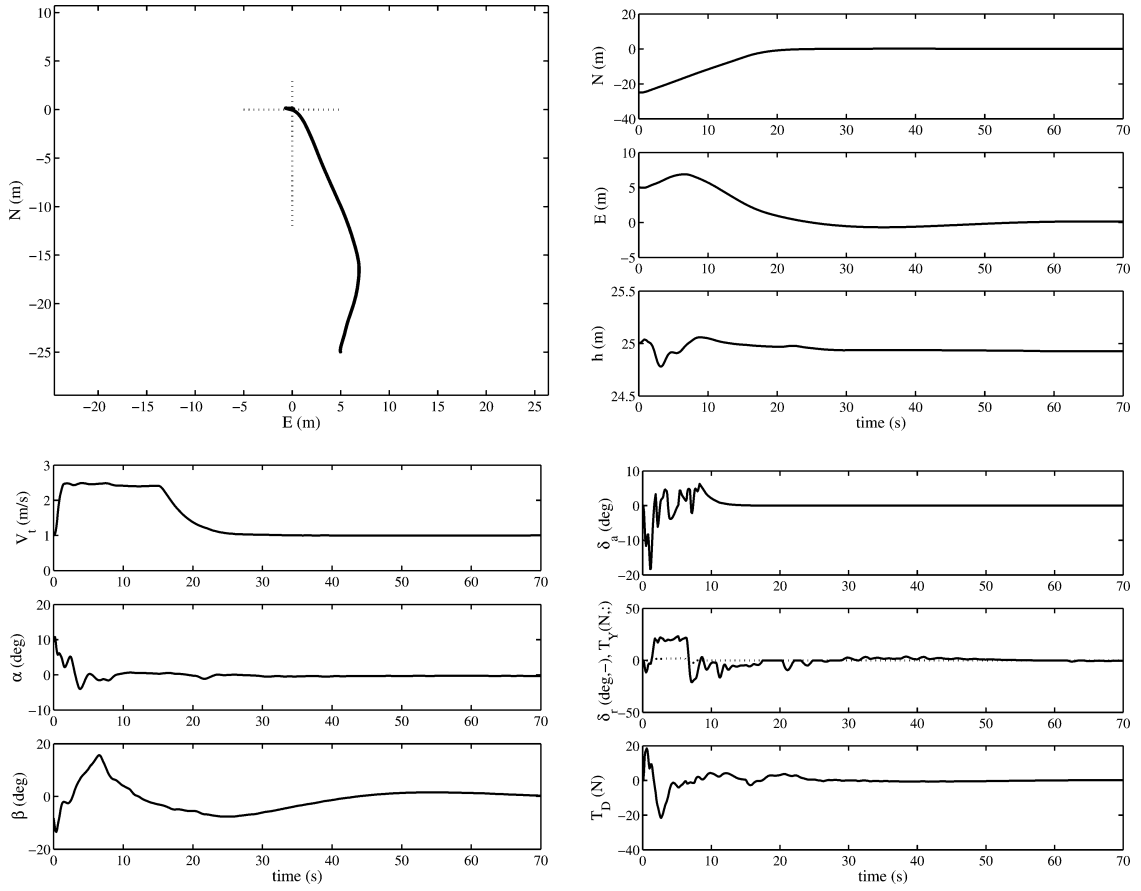

Fig. 7 Stabilization in low wind in the RA case.

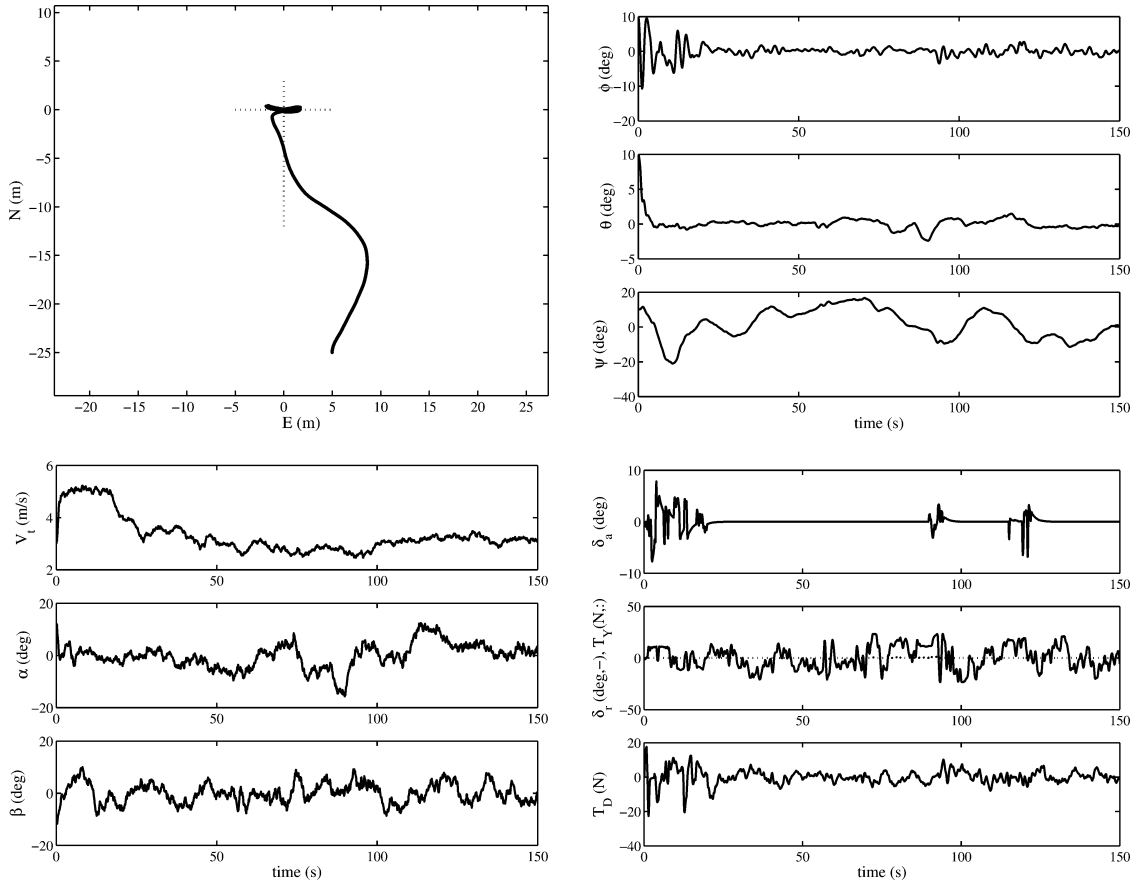

Fig. 8 Turbulent wind case.

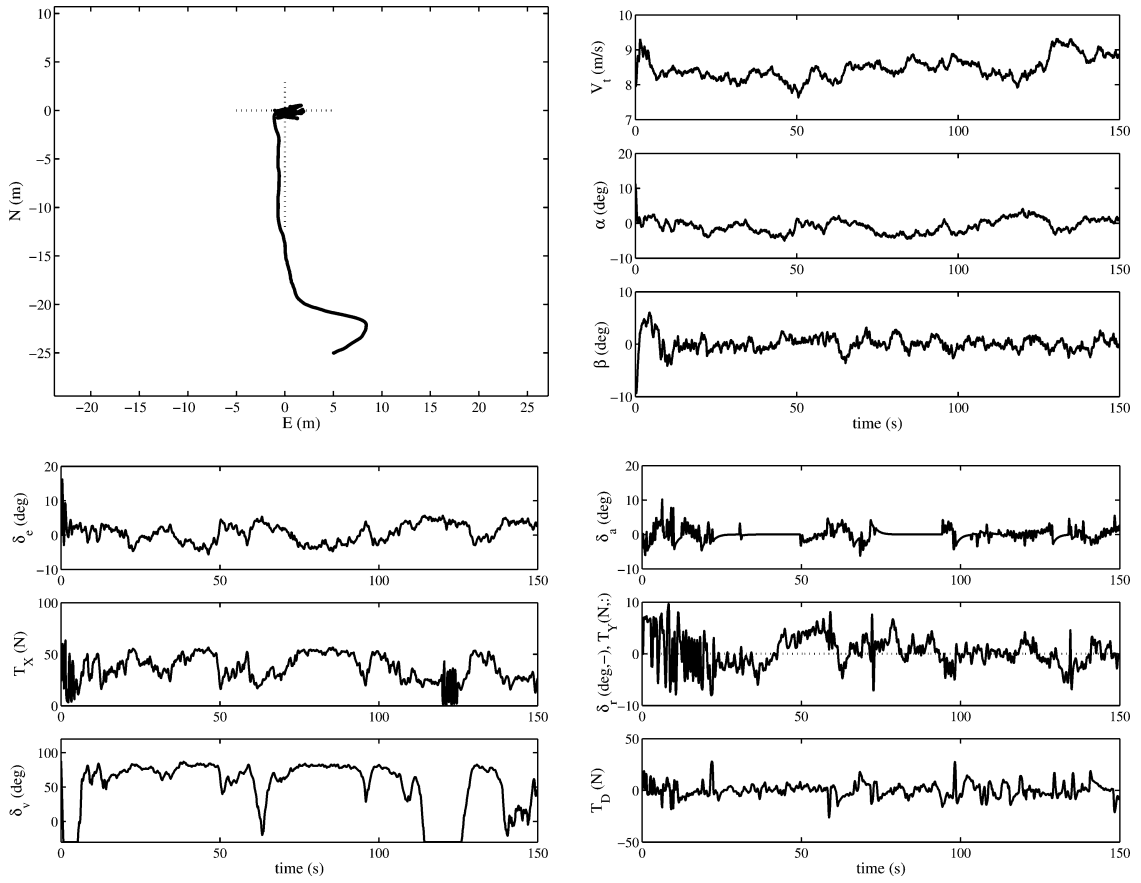

Fig. 9 Simulation in 8-m/s wind and turbulence.

Table 1 RMS values for hovering in 3- or 8-m/s wind and turbulence simulation (last 100 s)

Mean wind speed	N, cm	E, cm	h, cm	ϕ, deg	θ, deg	ψ, deg	V_t, m/s
3 m/s	20	114	5.8	0.9	0.7	8.5	0.23
8 m/s	41	95	45	4.1	0.9	2.3	0.63

results in Table 1. The values are in perfect agreement with the previous comments, and they confirm that the hovering stabilization is well achieved, despite the high turbulent disturbance. Namely the roll and pitch attitude angles are quite stable.

D. Increased Wind and Turbulence

Finally, to demonstrate the system behavior when the aerodynamic forces are significant and the tail authority is higher, a simulation was run with a mean wind of 8 m/s and a turbulent component with an intensity of 3 m/s. This simulation corresponds to a more difficult hover case because of the higher wind and increased forces to stabilize. At this airspeed, the increase in aerodynamics allows for higher forces and moments from the tail fins, such that the force maxima can now be considered as $[F_1, F_2, F_3, F_4, F_5, F_6] = [107, 29, 40, 59, 586, 59](N)$. In Fig. 9 some illustrative results of a 150-s simulation are presented, with the horizontal path, aerodynamic variables, and the control inputs. Comparing with the nominal wind case, one can easily note the noisy signals with a higher frequency. In this case, the longitudinal control seems more difficult, and the vectoring angle is clearly hesitating between the usual hover position, which would be vertical (90 deg) in smaller winds, and the cruising flight case, where the propellers would normally not be vectored. The interpretation of this case very obviously shows that for such an airspeed the airship should be controlled using the aerodynamic lift instead of the vectoring, and thus the reference pitch angle should no longer be zero. Keeping the hovering reference model implies a higher use of the propellers, when the elevators could be much more efficient.

Trying to quantify the quality of the hover stabilization in this illustrative case, the rms values of the last 100 s are here again computed and are also presented in Table 1. Comparing with the previous 3-m/s mean wind speed case, we verify that the lateral position control is better. On the other hand, the longitudinal variables (N, h) have now magnitude values similar to the lateral one. The pitch angle is however still very well stabilized.

VI. Conclusions

This paper introduces a novel approach for the problem of stabilizing an airship in hover. The main results of the work are outlined as 1) proposition of an original formulation of an airship kinematics/dynamics with an appropriate change of variable allowing the application of backstepping techniques; 2) design of a backstepping control strategy that stabilizes the hovering flight of the airship, which is robust against perturbations (wind and turbulence) and against unmatched dynamics; and 3) proposition of a theoretical study closely related to practical applications, as the actuators saturation is considered in the design. The backstepping approach used relies in a nonlinear combination of saturation functions of linear feedbacks ensuring global stabilization under saturation. The problem of actuator limits is of fundamental interest for this kind of underactuated systems; 4) and finally, the proposition of a guidance strategy to deal with the problem of the airship lateral underactuation. The strong lateral underactuation of the airship is dealt with using a modified control objective in order to make the airship follow a given reference path from the current state to the desired state reducing the need of lateral forces and also allowing the airship to align itself against the wind in the hovering condition. Illustrative results are presented for the hovering stabilization of the Aurora project airship, showing the behavior and robustness of the proposed solution in a wide range of wind and turbulence conditions. Extensive

simulations for the refinement and full validation of the hovering backstepping approach are being carried out in the AURORA development environment, prior to the implementation in the real airship for experimental purposes.

Appendix: Saturation Definition and Properties

The definitions presented hereafter are inspired on the definitions introduced by Teel[17] and permit the extension of the stability of the control solution to the case of reduced actuation.

Definition 1: As a particular case and extension of the linear saturation definition proposed by Teel,[17] let us introduce the elementwise nondecreasing saturation function $\boldsymbol{\sigma}:\mathbb{R}^n \to \mathbb{R}^n$, defined by a vector $\boldsymbol{m}$ of n positive values m_i, with $m_i > r > 0$, and such that

$$\forall z \in \mathbb{R}^n, \qquad \boldsymbol{\sigma}[z] = \Sigma z \tag{A1}$$

where the diagonal matrix Σ is defined by

$$|z_i| < m_i \Rightarrow \Sigma_i = 1, \qquad |z_i| \geq m_i \Rightarrow \Sigma_i = m_i/|z_i| \tag{A2}$$

Properties: It can easily be verified that the definition yields the following properties[17]:

$$\begin{cases} \forall z \in \mathbb{R}^n; z^T \boldsymbol{\sigma}[z] > 0 \\ \forall z \in \mathbb{R}^n; |\boldsymbol{\sigma}[z]| \leq R \\ |z| < r \Rightarrow \boldsymbol{\sigma}[z] = z \end{cases} \tag{A3}$$

where $|z| = \sqrt{(z^T z)}$ is the norm of vector z as defined in $\mathbb{R}^n$ and $R^2 = \sum_{i=1}^{n} m_i^2$.

Theorem 1: If $z^T v = 0$, then

$$z^T \boldsymbol{\sigma}[z + v] > 0 \tag{A4}$$

Proof: Because v is orthogonal to z, it can be expressed as $v = \Omega z$, where Ω is antisymmetric, and we then have

$$z^T \boldsymbol{\sigma}[z + v] = z^T \Sigma(z + \Omega z) = z^T \Sigma z + z^T \Sigma \Omega z$$

Considering the last term, because it is a scalar we have

$$z^T \Sigma \Omega z = (z^T \Sigma \Omega z)^T = -z^T \Omega \Sigma z$$

and then

$$z^T \Sigma(z + \Omega z) = \tfrac{1}{2} z^T [\Sigma(I + \Omega) + (I - \Omega)\Sigma] z$$

or

$$z^T \Sigma(z + \Omega z) = z^T X z$$

where X is a symmetric matrix with a positive diagonal, which leads to the presented result. □

Theorem 2: If two saturations $\boldsymbol{\sigma}_1$ and $\boldsymbol{\sigma}_2$ are defined, such that $R_1 < \frac{1}{2} r_2$, then

$$\forall (z_1, z_2) \in \mathbb{R}^n, \qquad |z_2| > \tfrac{1}{2} r_2 \Rightarrow z_2^T \boldsymbol{\sigma}_2[z_2 + \boldsymbol{\sigma}_1[z_1]] > 0 \tag{A5}$$

Proof: Because $|z_2| > \frac{1}{2} r_2$ and $|\boldsymbol{\sigma}_1[z_1]| \leq R_1 < \frac{1}{2} r_2$, and considering the orthogonal projection of the saturated vector on z_2, one can write

$$\boldsymbol{\sigma}_1[z_1] = \lambda_1 z_2 + v_1$$

where $|\lambda_1| < 1$, $z_2^T v_1 = 0$, and $|\lambda_1 z_2 + v_1| < \frac{1}{2} r_2$, leading to

$$|z_2 + \lambda_1 z_2 + v_1| < r_2$$

and then

$$\begin{aligned} z_2^T \boldsymbol{\sigma}_2[z_2 + \boldsymbol{\sigma}_1[z_1]] &= z_2^T \boldsymbol{\sigma}_2[(1 + \lambda_1) z_2 + v_1] \\ &= z_2^T \Sigma_2[(1 + \lambda_1) z_2 + v_1] \\ &= (1 + \lambda_1) z_2^T \Sigma_2 z_2 > 0 \end{aligned}$$ □

Corollary 1: If $|z_2| > \frac{1}{2} r_2$ and $|\boldsymbol{\sigma}_1[z]| < \frac{1}{2} r_2$, and $z_2^T v_2 = 0$, then

$$z_2^T \boldsymbol{\sigma}_2[z_2 + v_2 + \boldsymbol{\sigma}_1[z_1]] > 0 \tag{A6}$$

Proof: If

$$\boldsymbol{\sigma}_1[z_1] = \lambda_1 z_2 + v_1$$

then

$$z_2^T \boldsymbol{\sigma}_2[z_2 + v_2 + \boldsymbol{\sigma}_1[z_1]] = z_2^T \boldsymbol{\sigma}_2[(1 + \lambda_1) z_2 + v_2 + v_1]$$

which can be written as

$$(1 + \lambda_1) z_2^T \boldsymbol{\sigma}_2[z_2 + v]$$

which, using theorem 1 and $|\lambda_1| < 1$, leads to the desired result. □

Theorem 3: If $\lambda_1 > 1$, then for all $|z_2| < |z_1|$

$$(z_2 + z_1)^T (z_2 + \lambda_1 z_1) > 0 \tag{A7}$$

Proof: Because $|z_2| < |z_1|$, the orthogonal projection of z_2 on z_1 gives

$$z_2 = \lambda_2 z_1 + v_2$$

where $|\lambda_2| < 1$ and $v_2^T z_1 = 0$, leading to

$$\begin{aligned} (z_2 + z_1)^T (z_2 + \lambda_1 z_1) &= [(\lambda_2 + \lambda_1) z_1 + v_2]^T [(\lambda_2 + 1) z_1 + v_2] \\ &= (\lambda_2 + \lambda_1)(\lambda_2 + 1) z_1^T z_1 + v_2^T v_2 > 0 \end{aligned}$$ □

Acknowledgments

The present work was partly developed in the frame of project DIVA-POSI/SRI/45040/2002, approved by the Portuguese Ministry of Science FCT and POSI program, with support from FEDER European Fund. The work was also sponsored by the Brazilian agencies CNPq Under Grant 150181/2003-5, and Fapesp under Grant 04/13467-5.

References

[1] Cox, T. H., Nagy, C. J., Skoog, M. A., and Somers, I. A., "Civil UAV Capability Assessment—Draft Version," NASA, Dec. 2004, URL: http://www.nasa.gov/centers/dryden/pdf/111761main_UAV_Capabilities_Assessment.pdf.

[2] Cambone, S. A., Krieg, K., Pace, P., and Wells, L., II, "Unmanned Aircraft Systems Roadmap 2005 20030," U.S. Dept. of Defense, Washington, DC, July 2005, URL: http://www.acq.osd.mil/usd/Roadmap%20Final2.pdf.

[3] Azinheira, J. R., Rives, P., Carvalho, J. R. H., Silveira, G. F., de Paiva, E. C., and Bueno, S. S., "Visual Servo Control for the Hovering of an Outdoor Robotic Airship," *Proceedings of the IEEE International Conference on Robotics and Automation*, Vol. 3, IEEE Publications, Piscataway, NJ, May 2002, pp. 2787–2792.

[4] Shim, H., Koo, T. J., Hoffmann, F., and Sastry, S., "A Comprehensive Study of Control Design for an Autonomous Helicopter," *Proceedings of the 37th IEEE Conference on Decision and Control*, Vol. 4, IEEE Publications, Piscataway, NJ, Dec. 1998, pp. 3653–3658.

[5] Guo, L., Melhuish, C., and Zhu, Q.,"Towards Neural Adaptive Hovering Control of Helicopters," *Proceedings of the IEEE International Conference on Control Applications*, Vol. 1, IEEE Publications, Piscataway, NJ, Sept. 2002, pp. 54–58.

[6] Yang, C.-D., and Liu, W.-H., "Nonlinear H_∞ Decoupling Hover Control of Helicopter with Parameter Uncertainties," *Proceedings of the American Control Conference*, Vol. 4, IEEE Publications, Piscataway, NJ, June 2003, pp. 3454–3459.

[7] Mahony, R., Hamel, T., and Dzul A., "Hover Control via Lyapunov Control for an Autonomous Model Helicopter," *Proceedings of the 38th Conference on Decision and Control*, Vol. 4, IEEE Publications, Piscataway, NJ, Dec. 1999, pp. 3490–3495.

[8]Metni, N., Hamel, T., and Derkx, F., "A UAV for Bridges' Inspection: Visual Servoing Control Law with Orientation Limits," *Proceedings of the 5th IFAC/EURON Symposium on Intelligent Autonomous Vehicles*, Vol. 1, Elsevier, New York, July 2004.

[9]Ramos, J. J. G., de Paiva, E. C., Azinheira, J. R., Bueno, S. S., Maeta, S. S., Mirisola, L. G. B., and Bergerman, M., "Autonomous Flight Experiment with a Robotic Unmanned Airship," *IEEE International Conference on Robotics and Automation—ICRA'2001*, Vol. 1, IEEE Publications, Piscataway, NJ, May 2001, pp. 4152–4157.

[10]Bueno, S. S., Azinheira, J. R., Ramos, J. G., de Paiva, E. C., Carvalho, J. R. H., Elfes, A., Rives, P., and Silveira, G. F., "Project AURORA: Towards an Autonomous Robotic Airship," *Workshop on Aerial Robotics, IEEE International Conference on Intelligent Robots and Systems*, Vol. 1, IEEE Publications, Piscataway, NJ, Oct. 2002, pp. 43–54.

[11]Khalil, H. K., *Nonlinear Systems*, 3rd ed., Prentice–Hall, NJ, Chap. 14, 2002, pp. 589–603.

[12]Kim, K.-S., and Kim, Y., "Robust Backstepping Control for Slew Maneuver Using Nonlinear Tracking Function," *IEEE Transactions on Control Systems Technology*, Vol 11, No. 6, 2003, pp. 822–829.

[13]Hygounenc, E., and Soueres, P., "Automatic Airship Control Involving Backstepping Techniques," *Proceedings of the IEEE International Conference on Systems, Man and Cybernetics*, Vol. 6, IEEE Publications, Piscataway, NJ, Oct. 2002, pp. 1–6.

[14]Frazzoli, E., and Dahleh, M. A., and Feron, E., "Trajectory Tracking Control Design for Autonomous Helicopters Using a Backstepping Algorithm," *Proceedings of the American Control Conference*, Vol. 6, IEEE Publications, Piscataway, NJ, 2000, pp. 4102–4107.

[15]Beji, L., Abichou, A., and Bestaoui, Y.,"Stabilization of a Nonlinear Underactuated Autonomous Airship—a Combined Averaging and Backstepping Approach," *Proceedings of the Third International Workshop on Robot Motion and Control*, Vol. 1, IEEE Publications, Piscataway, NJ, Sept. 2002, pp. 223–229.

[16]Toussaint, G. J., Basar, T., and Bullo, F., "Tracking for Nonlinear Underactuated Surface Vessels with Generalized Forces," *Proceedings of the IEEE International Conference on Control Applications*, Vol. 1, IEEE Publications, Piscataway, NJ, Sept. 2000, pp. 355–360.

[17]Teel, A. R., "Global Stabilization and Restricted Tracking for Multiple Integrators with Bounded Controls," *Systems and Control Letters*, Vol. 18, No. 3, 1992, pp. 165–171.

[18]Freeman, R., and Praly, L., "Integrator Backstepping for Bounded Controls and Control Rates, *IEEE Transactions on Automatic Control*, Vol. 43, No. 2, 1998, pp. 258–262.

[19]de Paiva, E. C., Bueno, S. S., Gomes, S. B. V., Ramos, J. J. G., and Bergerman, M., "A Control System Development Environment for AURORA's Semi-Autonomous Robotic Airship," *Proceedings of the IEEE International Conference on Robotics and Automation*, Vol. 3, May 1999, pp. 2328–2335.

[20]Azinheira, J. R., de Paiva, E. C., and Bueno, S. S., "Influence of Wind Speed on Airship Dynamics," *Journal of Guidance, Control, and Dynamics*, Vol. 25, No. 6, 2002, pp. 1116–1124.

[21]Stevens, B. L., and Lewis, F. L., *Aircraft Control and Simulation*, Wiley, New York, Chap. 1, 1992, pp. 33–47.